Development of wake meandering detection algorithms and their application to large eddy simulations of an isolated wind turbine and a wind farm

IOP Conf. Series: Journal of Physics: Conf. Series **1037** (2018) 072024 doi:10.1088/1742-6596/1037/7/072024

Development of wake meandering detection algorithms and their application to large eddy simulations of an isolated wind turbine and a wind farm

N Coudou[1,2,3], M Moens[3], Y Marichal[4], J Van Beeck[2], L Bricteux[1], and P Chatelain[3]

[1] Mechanical Engineering Department, Université de Mons, 7000 Mons, Belgium
[2] von Karman Institute for Fluid Dynamics, Rhode-Saint-Genèse, Belgium
[3] Institute of Mechanics, Materials and Civil Engineering, Université catholique de Louvain, 1348 Louvain-la-Neuve, Belgium
[4] WaPT - Wake Prediction Technologies, 1348 Louvain-la-Neuve, Belgium

E-mail: nicolas.coudou@vki.ac.be

Abstract. We investigate several algorithms to detect the centerline of a wind turbine wake. First, we apply these methods during Large Eddy Simulations of an isolated wind turbine subject to a uniform ($TI = 0\%$) and a synthetic turbulent inflow ($TI = 10\%$). The simulations are performed using a vortex-particle mesh method with the blades modeled using immersed lifting lines. The most robust algorithm is then applied to investigate the wakes positions inside a wind farm. At wind farm scale, the simulations are performed with a fourth-order finite difference code inside which the wind turbines are accounted for through advanced actuator disks.

1. Introduction

Wind turbine wake meandering is a critical issue in wind farms as this oscillatory motion of the wakes increases fatigue loads on downstream machines and impacts their power production. The first step to study and model this phenomenon is to detect the wake centerlines inside measurements or high-fidelity simulations. Several methods are used in the literature [1, 2, 3, 4], usually to detect the position of the wake for turbines in yaw. In this work, we compare several techniques based on linear/angular impulse, velocity/momentum deficit and available power in the flow for run-time tracking of the wake centerline during Large Eddy Simulations (LES) of the NREL offshore 5-MW baseline wind turbine subject to a uniform inflow and to a synthetic turbulent inflow. The simulations are performed with a state-of-the-art Vortex Particle-Mesh (VPM) method combined with immersed lifting lines [5, 6, 7]. The most robust technique is then applied at wind farm scale thanks to the use of a fourth-order finite difference [8] code inside which the machines are modeled with advanced Actuator Disks (AD).

2. Methodology

2.1. The Vortex Particle-Mesh method

The Vortex Particle-Mesh method [5, 6, 7, 9] relies on the discretization of the velocity ($\mathbf{u}$)-vorticity ($\boldsymbol{\omega} = \nabla \times \mathbf{u}$) formulation of the incompressible Navier-Stokes equations in a Lagragian form. In this method, the vorticity field is discretized with particles which are used solely for the advection treatment, thereby avoiding dispersion errors and waiving classical time stability constraints (CFL number). The use of a mesh along with the particles in the VPM method offers several advantages. The mesh enables the treatment of the Lagrangian distortion through the periodic regularization onto the grid of the particles set [9]. In addition, the mesh handles the computationally intensive tasks : the evaluation of differential operators and the use of fast Poisson solvers for the computation of velocity. Both discretizations communicate through high order interpolation.

This method is able to solve complex turbulent flows at high Reynolds number by using a LES approximation with a Regularized Variational Multiscale (RVM) subgrid-scale model [10] designed as an eddy viscosity model acting only on the small scales.

2.1.1. Blades modeling through immersed lifting lines The generation of vorticity along the rotor blades is accounted for through immersed lifting lines. Under the assumption of slender blades, a blade can be approximated as a concentrated bound vortex going through the quarter-chord line, and treat the flow around the airfoil in a section as essentially two-dimensional. For a steady flow, the lift per unit span $\mathbf{L}$ and the bound circulation $\mathbf{\Gamma}(r,t)$ are then related by the Kutta-Joukowski theorem

$$\mathbf{L} = \rho \mathbf{V}_{rel} \times \mathbf{\Gamma} \tag{1}$$

where ρ is the air density and $\mathbf{V}_{rel} = \mathbf{u} - \mathbf{u}_{blade}$ is the velocity relative to the blade. The lift can also be obtained from the relative velocity and the airfoil lift behavior, through its C_L coefficient –either static or in a dynamic stall model; this allows to compute the bound circulation $\mathbf{\Gamma}(r,t)$ as well as the shed vortex sheet from the solenoidal property of $\boldsymbol{\omega}$.

2.1.2. Turbulent inflow A turbulent velocity field $\mathbf{u}'$ is synthesized through Mann's algorithm [11]. In order to carry the turbulence into the domain through the inflow plane, this turbulent velocity field is translated into a set of vorticity particles, more adequate for the Lagrangian method used. Note that because of the unbounded conditions in the $y-$ and $z-$directions, this initially periodic velocity field is made compact through a smooth clipping along its edges.

2.2. Fourth-order finite difference code

The VPM approach is well suited for high-fidelity and high-resolution simulations of an isolated wind turbine. However, this becomes unaffordable for simulations at the wind farm scale and another approach is required for investigating wind farm flows. We here consider LES on coarse meshes, performed using a fourth-order finite difference code [12]. The wind turbines are modeled with advanced AD, which account for thrust and torque effects; these disks also use the local prevailing velocities at every point of the AD for the computation of the aerodynamic loads [8, 13]. The model has been supplemented with a tip-loss correction based on a local estimation of the effective upstream velocity at every point of the AD [13].

Instantaneous velocities are imposed at the inlet boundary and a convective boundary condition is applied at the outflow. Periodic boundary conditions are imposed in the spanwise direction and no-through flow is enforced at the top. A wall stress model for a rough wall is applied at the bottom; it relies on a roughness length, y_0 and the velocity evaluated at the third grid point. In the present simulations, turbulent inflow conditions are obtained with a precursor simulation. This involves running a prior simulation without wind turbines, driven by

a prescribed pressure gradient, $\frac{1}{\rho}\frac{\partial p}{\partial x} = \frac{u_\tau^2}{H}$, depending on the friction velocity u_τ and the height of the boundary layer H. yz-planes of instantaneous velocities are saved, to be later used as inflow for the main simulations with the turbines.

2.3. Wake centerline diagnostics

The proposed diagnostics take advantage of the specific signatures of a wind turbine wake, namely its vortical structures, the deficits of mass flow, momentum, and available power in the flow. The first investigated techniques rely on the moments of vorticity in a cross-flow plane, i.e. the densities of linear and angular impulse, along and about $\mathbf{e}_x$, i_x and l_x

$$i_x = \frac{1}{2}\left(\mathbf{x}\times\boldsymbol{\omega}\right)\cdot\mathbf{e}_x\,,\ l_x = \frac{1}{3}\left(\mathbf{x}\times\left(\mathbf{x}\times\boldsymbol{\omega}\right)\right)\cdot\mathbf{e}_x. \tag{2}$$

One can also use the analogy with the displacement and momentum thicknesses of a boundary layer [14] and exploit the densities of the deficits of velocity/momentum in a cross-flow plane in the wake

$$s_1 = U_\infty - u_x\,,\ s_2 = \left(U_\infty - u_x\right)u_x. \tag{3}$$

From one of these densities $q = i_x, l_x, s_1, s_2$, the centroid of the wake can be obtained in every plane normal to the streamwise direction by computing the first moment of the density q [4]

$$y_c = \frac{\int y\,q\,dS}{\int q\,dS}\ ,\ z_c = \frac{\int z\,q\,dS}{\int q\,dS}. \tag{4}$$

Given the deficit of available energy in the wake of a wind turbine, a diagnostic based on the available power density in the wake is also assessed. This method relies on the computation of the wind power inside a disk of a diameter equal to the rotor diameter D and located in a cross-flow plane. This disk center position can be shifted in the $y-$ and $z-$directions; the wake center then corresponds to the disk position for which the available power is minimum [3]. Practically, this method consists in locating the maximum of the convolution

$$\left(y_c, z_c\right) = \mathrm{argmax}\left(p * f_s\right) \tag{5}$$

between the available power density $p(y,z) = \frac{1}{2}u_x|\mathbf{u}|^2$ and a masking function f_s set to minus unity inside the rotor disk and to zero outside of it

$$f_s(y,z) = \begin{cases} -1 \text{ if } y^2 + z^2 < \left(\frac{D}{2}\right)^2, \\ 0 \text{ otherwise.} \end{cases} \tag{6}$$

The robustness displayed by the convolution method (see Section 3.1.2 in particular) motivated the investigation of further potential refinements of this technique. First, the convolution was also performed using the densities of velocity/momentum deficit (Eq. 3) in the wake to study the influence of the field density on the wake centerline location. Furthermore, the influence of the mask function was investigated by replacing the discontinuous filter function by a Gaussian function

$$f_g(y,z) = A\,\exp\left(-\left(\frac{(y-\mu_y)^2}{2\sigma_y^2} + \frac{(z-\mu_z)^2}{2\sigma_z^2}\right)\right) \tag{7}$$

with $A = -1$, $\mu_{y,z} = 0$, and $\sigma_{y,z} = D/4$. Finally, the influence of the mask size was studied for the Gaussian function. Instead of testing several $\sigma_{y,z}$, a method to perform an automatic adaptation of $\sigma_{y,z}$ according to space and time was developed. It exploits the property that the

Laplacian of the convolution between two gaussian functions is minimum when their $\sigma_{y,z}$ are equal. Therefore, two additional convolutions were computed for mask widths corresponding to $\sigma_{y,z} = \sigma_{y,z} \pm d\sigma_{y,z}$. The convolution with the narrower extremum was then selected by comparing the Laplacians computed at the position of the extrema and the wake centroid was determined from the position of the narrower extremum. Note that $\sigma_{y,z} = D/4$ was selected as first guess to show that our adaptation algorithm of $\sigma_{y,z}$ is robust even if the initial guess is not optimal ($\sigma_{y,z} = D/2$ would have been a better guess).

In order to obtain the wake centerline, these techniques are applied in each cross-flow plane (depending on the mesh resolution) in the wake of a machine.

3. Results

The diagnostics presented in Section 2.3 are first applied to the wake of an isolated wind turbine subject to a uniform and a turbulent inflow, and then to the wakes of a 3×5 wind farm subject to a turbulent inflow.

3.1. Isolated wind turbine

The LES computations are performed for the NREL offshore 5-MW baseline wind turbine [15] operating at its optimum tip-speed ratio $TSR = 7.55$. Only the blades of the wind turbine are modeled using immersed lifting lines. The spatial resolution is such that 32 points are used to model each blade. The computational domain initially extends over $14D \times 4D \times 4D$; the domain is unbounded in $y-$ and $z-$directions. Based on the spatial resolution of the blades, it leads to an initial grid with approximately 59 million nodes. The wind turbine rotor is located $3D$ after the inlet and is subjected to both a uniform and a turbulent wind. The inflow velocity is $U_\infty = 9$ ms^{-1} in the $x-$direction and the turbulence intensity $TI = u'/U_\infty = 0\%$ and $TI = 10\%$. The turbulent field is synthesized through Mann's algorithm and fills a $26D \times 4D \times 4D$ box.

The simulations were performed on 512 processors with a typical time-to-solution of at most 12 hours, thus hinting at the good efficiency of the computational method. The wake centerline diagnostics were started after one flow-through time $t^* = L_x/U_\infty$.

3.1.1. Uniform inflow The diagnostics presented in Section 2.3 are first applied to the wake of an isolated wind turbine subject to a uniform inflow. The techniques based on the linear and angular impulses lead to a noisy wake centerline while the other techniques provide a wake centerline that remains close to the rotational axis of the rotor, as expected for a uniform inflow ($TI = 0\%$). For the sake of brevity, the figures for the uniform inflow are not presented in this article.

3.1.2. Turbulent inflow The diagnostics are now applied to a simulation with a turbulent inflow ($TI = 10\%$). The techniques based on the linear and angular impulses are too sensitive to the ambient turbulence and give incorrect wake centerlines. As it can be observed on Fig. 1, the other evaluated methods allow to track the wake motion quite properly. Nevertheless, the wake centerline location obtained with the methods based on the computation of the first order moment (Eq. 4) of the field density depend on the size of the surface on which the field density is integrated; the method based on the convolution is therefore much more robust.

The influence of the density field used in the convolution method was then investigated by applying the convolution method to the velocity/momentum deficit densities instead of the available power density. Figure 2a shows that the change in the type of density field does not have a significant impact on the wake centerline localization. As shown in Fig. 2b,c,d, the shape of the masking function, i.e. the discontinuous masking function (Eq. 6) vs a continuous one

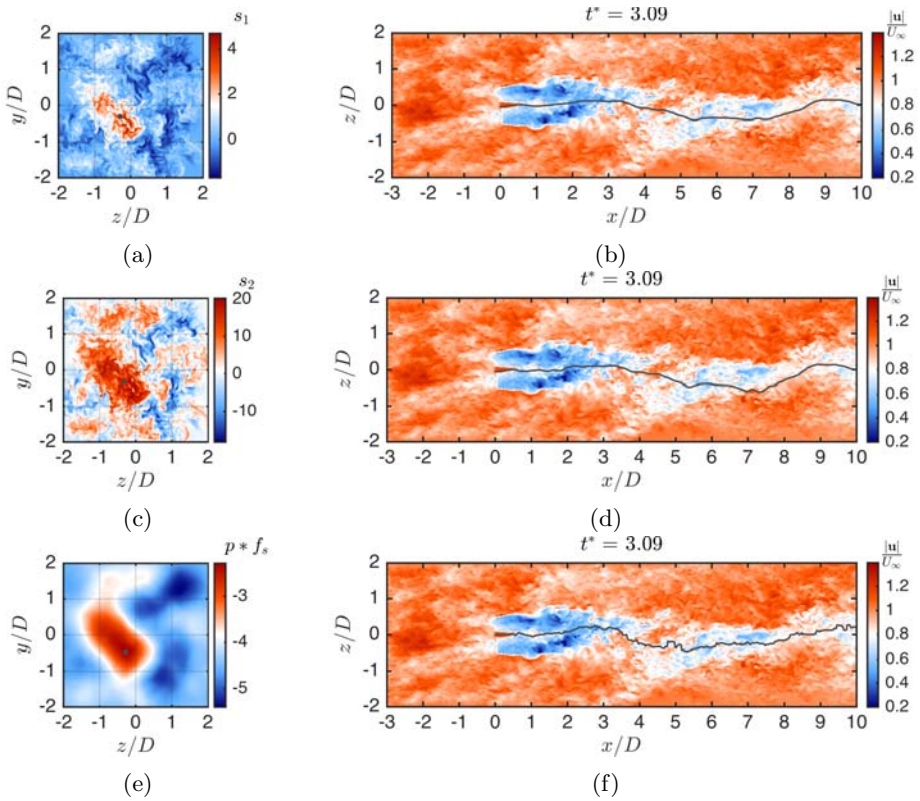

Figure 1: Assessment of wake centerline tracking at $TI = 10\%$. Snapshots, in a cross-flow slice located at $x/D = 5$, of diagnostic quantities (*left*) and, in a horizontal plane located at hub height, of dimensionless velocity magnitude (*right*) on which is superimposed the wake position obtained with the diagnostic based on the velocity deficit (a-b), momentum deficit (c-d), and convolution between a disk of diameter D and the density of available power (e-f)

(Eq. 7) plays a greater role (even if still limited) in the behavior of the detection algorithm than the nature of the density field used. Not too unexpectedly, the wake centerlines obtained with the Gaussian mask appear smoother than the ones obtained with the disk. The Gaussian mask however does not appear to reduce the amplitude of the large-scale wake oscillations.

Next, the influence of the mask size was investigated for the Gaussian function. As presented in Section 2.3, an automatic adaptation of $\sigma_{y,z}$ (Eq. 7) was implemented in order to replace the use of $\sigma_{y,z}$ values that have to be prescribed a priori. Figure 3 shows the evolution of $\sigma_{y,z}$ as a function of space at two instants. As it can be observed on Fig. 3a, the mask size increases as a function of space because of the wake expansion. Note that the peaks observed in Fig. 3b can be traced to unsteadiness in the very generation of the wake at the wind turbine and, as a result, an irregular wake structure. Figure 4a,b,c shows that the mask size adaptation has almost no influence on the wake centerline localization. Nevertheless, this automatic adaptation of the mask size can be used to obtain the wake borders, another crucial value that needs to be predicted by operational models. These wake borders are shown in Fig. 4d: we set these borders to $\pm 1.35\sigma_{y,z}$ from the wake centerline position obtained with the velocity deficit density field.

Figure 5 shows the dimensionless horizontal motion of the wake centerline as a function of space and time. As it can be observed, the meandering amplitude increases as a function of space. The preliminary spectral analysis performed in time and in space results in a frequency $f = 8.5 \cdot 10^{-3}$ Hz and a wave number $k = 0.01$ rad m^{-1}. From this frequency and the wavelength

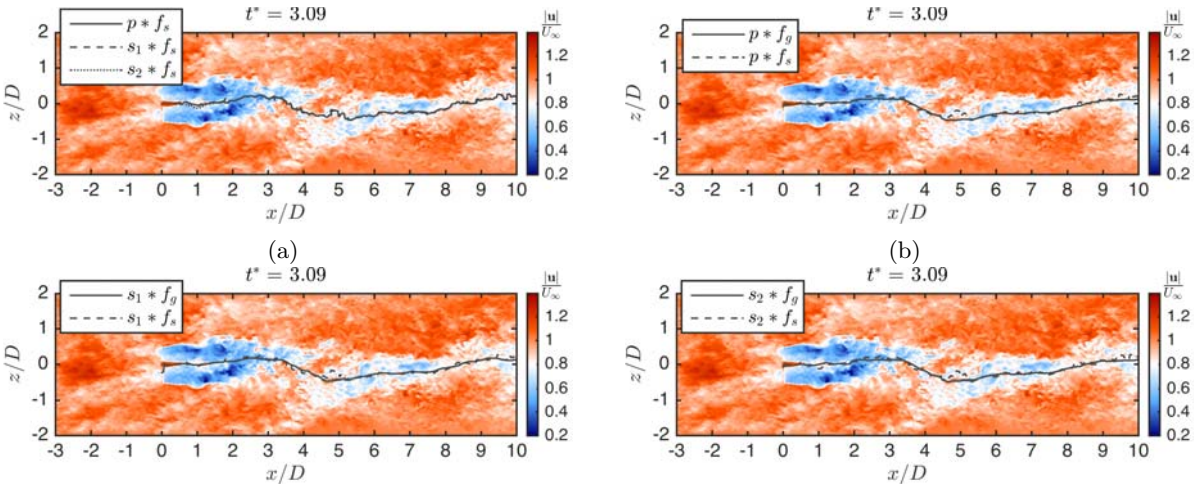

Figure 2: Dimensionless velocity magnitude in a horizontal plane located at hub height for $TI = 10\%$ together with the wake centerline obtained with the method based on the convolution between a circular mask of a diameter D and the densities of power, velocity deficit and momentum deficit (a), and with the method based on the convolution between a circular/gaussian mask of a diameter D and the densities of power (b), velocity deficit (c) and momentum deficit (d)

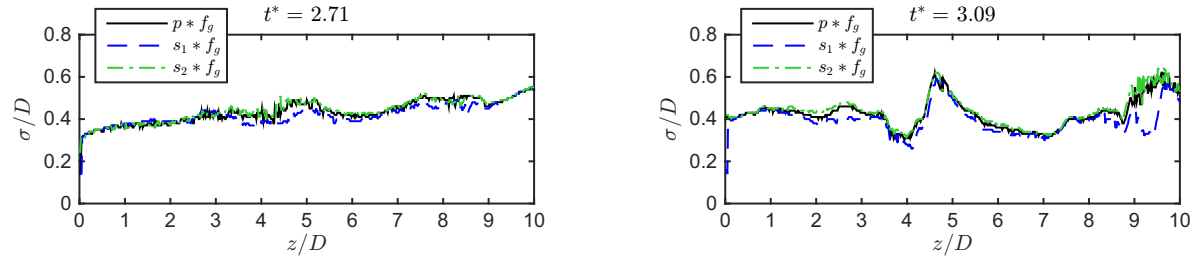

Figure 3: $\sigma_{y,z}$ as a function of space at two instants

$\lambda = 2\pi/k = 631$ m, or 5 rotor diameters, the phase velocity of the meandering was computed $u_p = \lambda f = 5.4$ m s^{-1}, or 59.5% of the average freestream velocity U_∞. This value is close to the speed of the vortex sheet $u_{vs} = 1/2\,(U_\infty + 1/3\,U_\infty) = 2/3\,U_\infty = 6$ m s^{-1}.

3.2. Wind farm

We perform some preliminary investigations inside a wind farm. Again, we consider the NREL-5MW machine; the wind turbine model is here supplemented with generator-torque and blade-pitch controllers [15] and a yaw control scheme [16].

The global domain size is $52D \times 8D \times 28D$ with a resolution of 16 points per D in the horizontal directions, and 32 points per D in the vertical direction ($\Delta x = \Delta z \simeq 7.88$, and $\Delta y \simeq 3.94$). The wind farm is arranged with 3 lines of 5 machines, with a distance of $7\,D$ between each rotor in both directions. The first wind turbines are located at $14D$ from the inlet and the hub height is located at 90 m [15]. The inflow conditions are obtained with a precursor simulation, performed on a domain of the same size as the main simulation, but with a coarser resolution (12 points per D in the vertical direction and 6 points per D in x and z directions). y_0 and u_τ are 0.1 and 0.25 m s^{-1}, respectively, which lead to an average hub velocity, U_{hub}, of

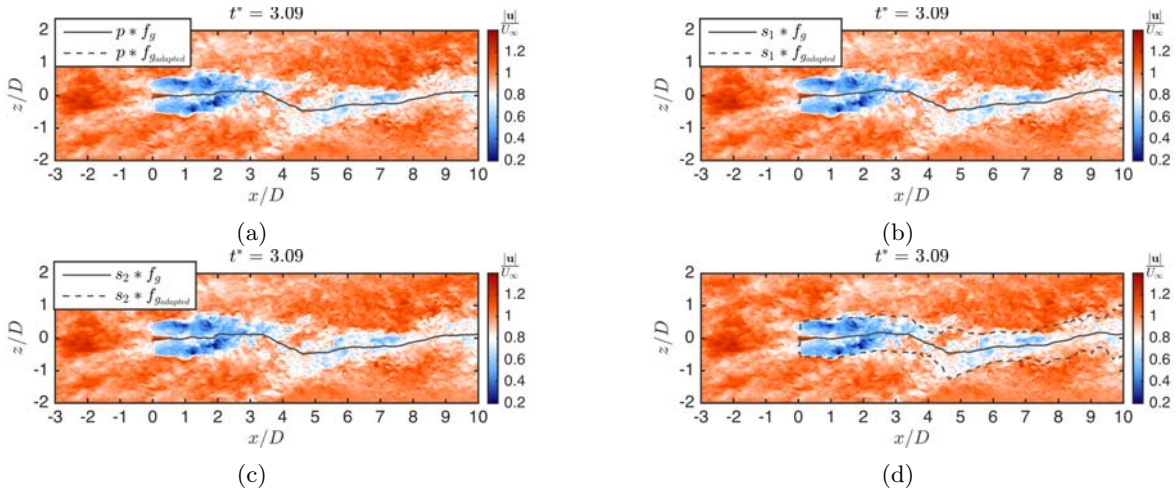

Figure 4: Dimensionless velocity magnitude in a horizontal plane located at hub height for $TI = 10\%$ together with the wake centerline obtained with the method based on the convolution between a Gaussian mask of $\sigma_{y,z} = D/4$ and of varying $\sigma_{y,z}$ and the densities of power (a), velocity deficit (b) and momentum deficit (c), and together with the wake borders obtained from the method based on the convolution between a Gaussian mask of varying $\sigma_{y,z}$ and the density of velocity deficit (d)

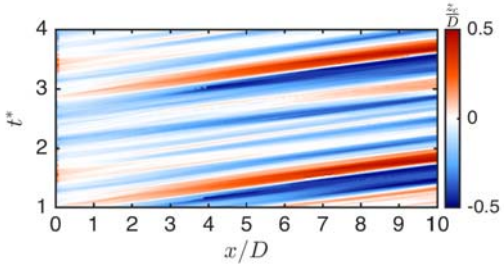

Figure 5: Dimensionless horizontal motion of the wake centerline as a function of space and time obtained with the method based on the convolution between the available power density and a Gaussian function with adapted $\sigma_{y,z}$

9 m s^{-1} and a TI of about 6 %. The time-step is set to 0.125 s.

For these simulations, the wake meandering tracking has been investigated in a post-processing step. The 3-dimensional velocity field has been saved every 2 seconds for a period of 728 s, corresponding to $T = 52D/U_{hub}$; the storage starts after $2T$). As the distance between the lowest part of the disk (and so the wake) and the ground is very small, the domain has been artificially increased in the vertical direction by symmetrizing the field below the wall; this allows to use the 2D convolution through the all vertical length around the wind turbine.

The chosen technique is here a convolution between the available power and a circular mask. However, some problems arise due to the presence of the ground and the relatively small clearance for the lowest point of the disk. The convolution really smooths the field, and minimal values are found near the ground; this mostly happens at a certain distance behind the rotor, where the wake is less structured (see Fig. 6). Globally, the wake meandering in the vertical direction is thus less well captured than that in the horizontal direction. However, the wake movement in the vertical direction is constrained by the ground and its magnitude is less important than that of the wake meandering in the z-direction (see Fig. 7): this movement direction is the crucial one for wake effects and their control through sideslip for instance. The proximity with the ground

also prevents the use of the method that adapts $\sigma_{y,z}$ based on the Laplacian computation at the minimum location. A larger σ_y indeed increases the influence of the ground on the convoluted field and eventually leads to the identification of a minimum in the very low velocity regions close to the ground. We could adapt σ_z only, but the approach is only valid when $\sigma_y = \sigma_z$. Moreover, the method cannot be transposed in 1 dimension, by minimizing the second derivative in the z-direction, because the value is minimum when σ_z is equal to $1/\sqrt{2}$ of that of the flow. We thus keep a circular mask for the first investigations. A solution for reducing the impacts of the ground effect in the wake meandering tracking algorithm could be to subtract the mean inflow velocity.

We clearly see that the wake movement increases for the downstream machines. This is better highlighted with the dimensionless horizontal wake movement, presented as a function of time and axial location, presented in Fig. 8 for the three lines of wind turbines. We clearly notice the influence of the downstream rotors on upstream wakes: the amplitude of the meandering decreases when the wake impacts another rotor and merges with the newly shed wake (vertical white areas at the first rotor positions; we will discuss the behavior of the last rotors in the next paragraph). The phase velocity also seems conserved since the pattern slopes do not seem affected by a merging event. By comparing the three different lines, the wake movement seems slightly lower for the central line; one potential explanation is a joint blocking effect by the two outer lines of turbines. This should however be confirmed in further investigations.

For this wind farm configuration, the algorithm only seeks one minimum per line. The amplitude thus always goes to zero at the rotor position. However, for the last rotors in the line, for example the fourth machine of the first line in Fig. 7a, the wake has a higher amplitude of oscillation and merges with the other wake at a further downstream position than that of the fifth rotor. We thus miss the remaining of the fourth wake, and the oscillations of this wake artificially disappear at the fifth wind turbine position. This also explains the strong change of the wake center location observed behind the fifth rotor of the first line (see Fig. 7b, at $z/D = 7$). The minimum available power detected by the algorithm does not correspond to the wake of the fifth machine but rather to the wake of the fourth one: this wake has not completely merged with the following one while being advected by the flow (see Fig. 7a and 7b). To improve the tracking, we plan to search for several minima in the wake of a machine in case of incomplete wake merging. A predictive method based on the estimation of the wake advection could be used to determine the region where the minimum/minima should be located.

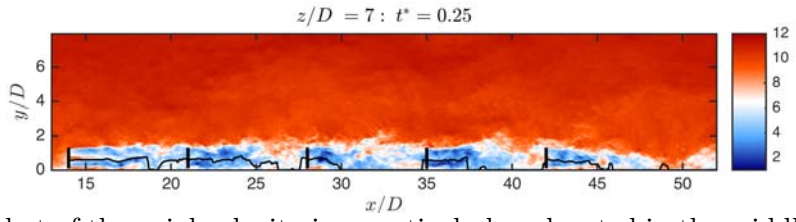

Figure 6: Snapshot of the axial velocity in a vertical plane located in the middle of the first line. The wake centerline is obtained with a convolution between the available power and a circular mask. The units are in [m s^{-1}] and the time is adimensionalized by the period T

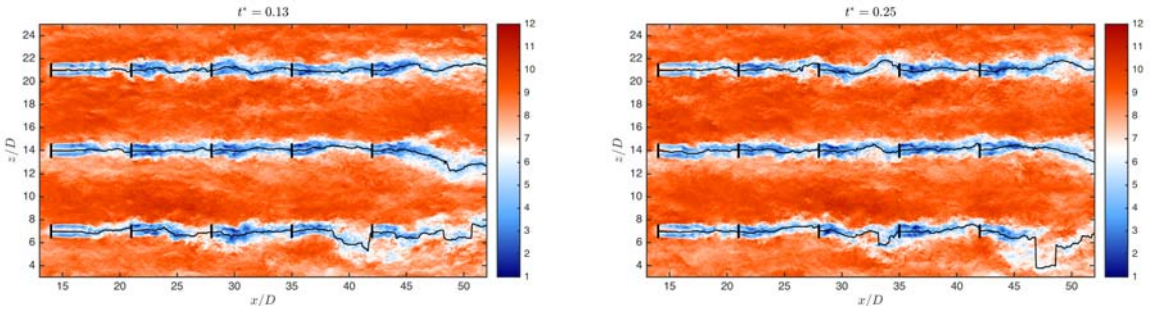

(a) (b)

Figure 7: Snapshot of the axial velocity in a horizontal plane located at hub height. The wake centerlines are obtained with a convolution between the available power and a circular mask. The units are in [m s^{-1}] and the time is adimensionalized by the period T

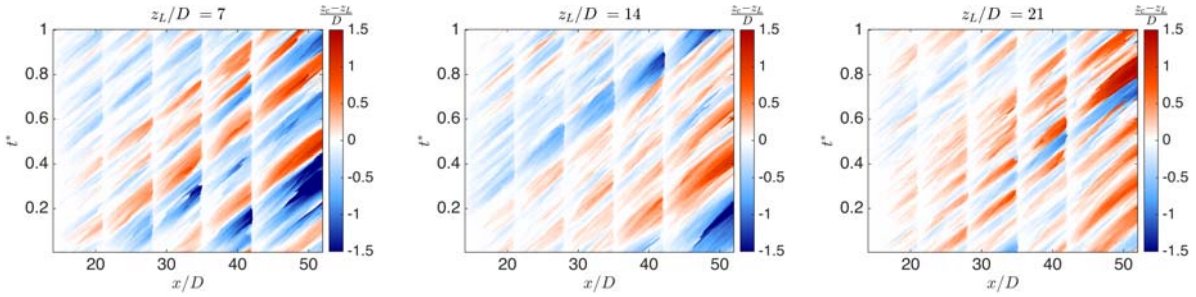

(a) (b) (c)

Figure 8: Dimensionless horizontal wake movement for the three lines of wind turbines, as a function of the adimensional time, $t^* = t/T$, and the adimensional axial position x/D

4. Conclusions and perspectives

In this work, several diagnostics were proposed to track the wake centerline of a wind turbine. These methods were first tested during LES computations of an isolated wind turbine subject to a uniform ($TI = 0\%$) and a turbulent inflow ($TI = 10\%$). The results indicate a good robustness for the technique based on a convolution. Additional investigations for this method highlight that the influence of the density field used in the convolution is weaker than the influence of the mask shape. The influence of the mask size was then investigated for the Gaussian function. Instead of testing several $\sigma_{y,z}$, a method to adapt $\sigma_{y,z}$ according to space and time was developed. Even if the adaptation of $\sigma_{y,z}$ has no major influence on the wake centerline localization, our results show that this method allows to capture the wake expansion and to track the wake borders.

The method based on the convolution between the available power density and a circular mask was then applied to track the wakes of a 3 x 5 wind farm. The present study has shown the potential of the tracking algorithm for the automated extraction of wake trajectories and the development of operational wake models for wind farms. Several wake characteristics have been extracted and the effects of crucial events such as wake-wind turbine interactions and wake merging have been identified on the amplitude of the wake meandering phenomenon. These results are preliminary however; this is mostly due to the tracking algorithms which could clear benefit from simple, and already identified, developments in terms of predictive smoothing and data structure strategies. They should then be able to handle complex wake interaction events and estimate wake widths within farms.

Access to databases of wake diagnostics, such as those produced by the present methodology,

should prove valuable in several respects. At a fundamental level, the study of turbulence effects on wake meandering will benefit from wake trajectory data and in particular, from the determination of the potential correlations between the machine loads, the ambient turbulence and the wake trajectory. At an operational level, the produced wake traces can support (1) the tuning and validation of operational wake models [17] and (2) a support to wake-detection for the development of turbine and farm-level control schemes and development work toward wake operational models.

Acknowledgments

Nicolas Coudou and Maud Moens are funded by the *Fonds pour la Formation à la Recherche dans l'Industrie et dans l'Agriculture (FRIA)*, Belgium. The simulations used computational resources made available on the Tier-1 supercomputer of the Fédération Wallonie-Bruxelles, infrastructure funded by the Walloon Region under the Grant Agreement No. 1117545

References

[1] Trujillo J J, Bingl F, Larsen G C, Mann J and Khn M 2011 *Wind Energy* **14** 61–75 ISSN 1099-1824
[2] Aubrun S, Tchouaké T F, España G, Larsen G, Mann J and Bingöl F 2012 *Progress in Turbulence and Wind Energy IV: Proceedings of the iTi Conference in Turbulence 2010* (Berlin, Heidelberg: Springer Berlin Heidelberg) ISBN 978-3-642-28968-2
[3] Vollmer L, Steinfeld G, Heinemann D and Kühn M 2016 *Wind Energy Science* **1** 129–141
[4] Howland M F, Bossuyt J, Martínez-Tossas L A, Meyers J and Meneveau C 2016 *Journal of Renewable and Sustainable Energy* **8** 043301
[5] Chatelain P, Curioni A, Bergdorf M, Rossinelli D, Andreoni W and Koumoutsakos P 2008 **197** 1296–1304
[6] Chatelain P, Backaert S, Winckelmans G and Kern S 2013 *Proceedings of The 9th International Symposium on Engineering Turbulence Modelling and Measurements (ETMM-9), June 6–8, 2012, Thessaloniki, Greece* (*Flow, Turbulence and Combustion* vol 91) ed Rodi W ERCOFTAC (Springer) pp 587–605
[7] Backaert S, Chatelain P and Winckelmans G 2015 *Symposium on Particle Methods in Fluid Dynamics, October 15-17 2012, DTU Copenhagen* (*Procedia IUTAM* vol 18) ed Walther J H (IUTAM) pp 1–7
[8] Moens M, Duponcheel M, Winckelmans G and Chatelain P 2016 *Journal of Physics: Conference Series* **753** 032053
[9] Winckelmans G 2004 *Encyclopedia of Computational Mechanics* vol 3 ed Stein E, De Borst R and Hughes T J (John Wiley and Sons)
[10] Jeanmart H and Winckelmans G 2007 **19** 055110 ISSN 1070-6631
[11] Mann J 1998 *Probabilistic Engineering Mechanics* **13** 269–282
[12] Duponcheel M, Bricteux L, Manconi M, Winckelmans G and Bartosiewicz Y 2014 *International Journal of Heat and Mass Transfer* **75** 470–482
[13] Moens M, Duponcheel M, Winckelmans G and Chatelain P *Wind Energy* Accepted for publication
[14] Pope S 2000 *Turbulent Flows* (Cambridge University Press) ISBN 9780521598866 URL `https://books.google.be/books?id=HZsTw9SMx-0C`
[15] Jonkman J, Butterfield S, Musial W and Scott G 2009 Definition of a 5-mw reference wind turbine for offshore system development Tech. Rep. NREL/TP-500-38060 National Renewable Energy Laboratory (NREL)
[16] Kooijman H J T, Lindeburg C, Winkelaar D and van der Hooft E 2003 Dowec 6 MW Pre-design: Aero-elastic modeling of the DOWEC 6 MW pre-design in PHATAS Tech. rep. DOWEC Dutch Offshore Wind Energy Converter 1997-2003 Public Reports Petten, the Netherlands
[17] Marichal Y, De Visscher I, Chatelain P and Winckelmans G 2017 *Journal of Physics: Conference Series* **854** 012030